Figure 2. Growth-inhibitory effect of NK012 and CPT-11 on bulky RCC tumors. I.v. administration of NK012 or CPT-11 was started when the mean tumor volumes of groups reached a massive 1,500 mm³. The mice were divided into test groups as indicated. *A*, representative of each group at day 15 in the Renca allograft model. *Arrows*, Renca allografts (*top*). Time profile of tumor volume in mice treated with NK012 or CPT-11 at indicated doses (*bottom*). Each group consisted of 10 mice. *Bars*, SD. *B*, the comparison of antitumor activities of CPT-11 and NK012 in SKRC-49 xenografts and Renca allografts. Representative of mice treated with NK012 at day 0 and day 21. Experiments were repeated twice with similar results. The mice at day 0 in the photograph belong to the group in the second experiment which started just at day 21 of the first experiment. *Arrows*, tumor grafts. The relative tumor volume values at day 21 to those at day 0 in each group set to 1 (*bottom*). Each group consisted of 10 mice.
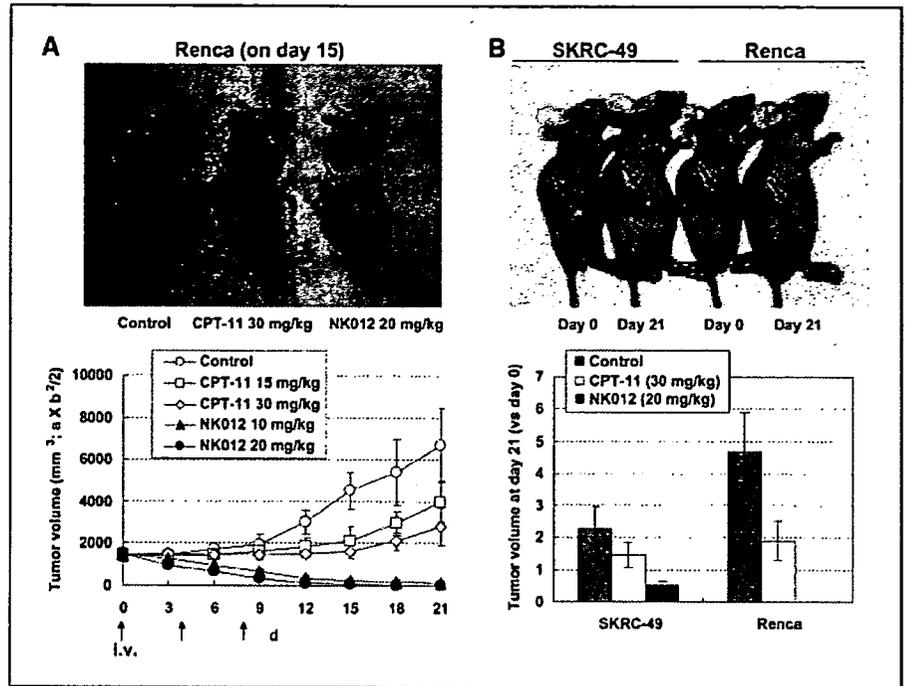
Fig. 3*B*). On the other hand, the concentrations of free SN-38 after administration of CPT-11 were almost negligible in metastatic lung tissues at all time points (data not shown). These results strongly suggest that SN-38 could be selectively released from NK012 and maintained in metastatic Renca tumor tissues.

Deviating from the ordinary experimental pulmonary metastasis prevention model, we initiated treatment 7 days after inoculation (day 0) when multiple lung nodules derived from Renca were observed in all mice in our preliminary study (Fig. 4*A*). On day 21, there was no significant difference between the mean number of

metastatic nodules in the control group (287 ± 56 nodules, $n = 10$) and in the group receiving CPT-11 treatment (236 ± 59 nodules, $n = 10$). Significant treatment effects were found, however, in the group receiving NK012 treatment (32 ± 18 nodules, $n = 10$) on day 21 compared with the control group on day 21 ($P < 0.0001$). Notably, a dramatic decrease in metastatic nodule number was observed in the NK012 treatment group on day 21 compared with the control group on day 0 (126 ± 23 nodules, $n = 10$, $P < 0.001$; Fig. 4*A*). Kaplan-Meier analysis showed that a significant survival benefit was obtained in the NK012 treatment group compared with
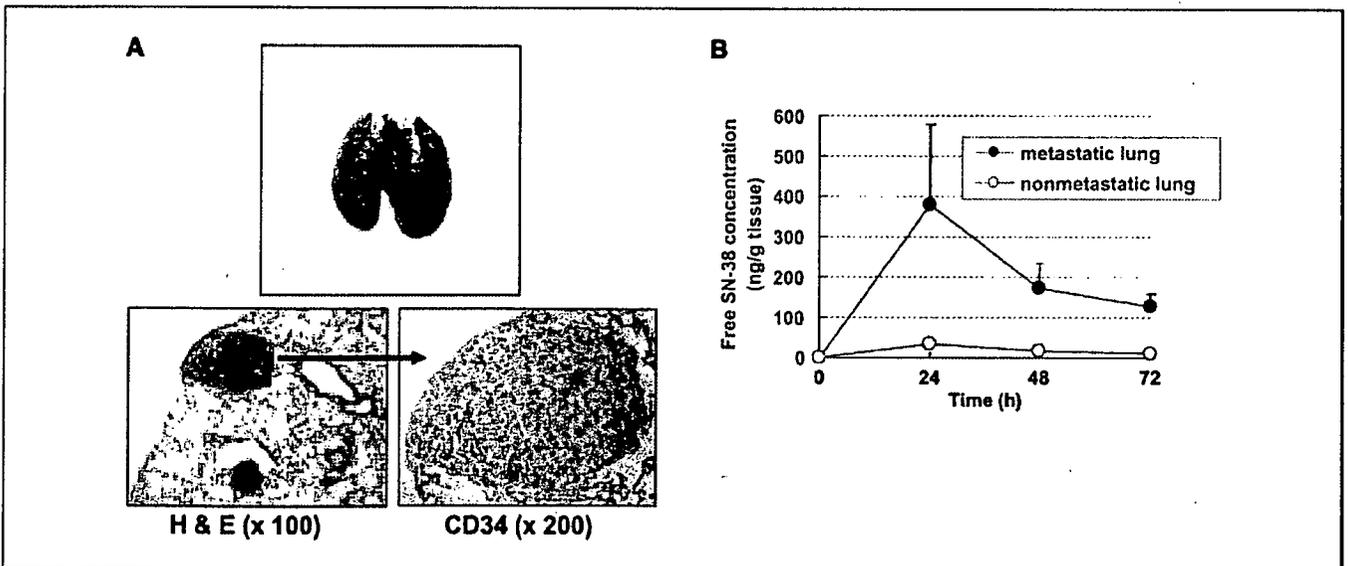

Figure 3. Pulmonary metastasis of Renca cells and lung tissue distribution of free SN-38 after administration of NK012 and CPT-11. *A*, gross appearances of pulmonary metastasis observed 7 d after Renca inoculation (*top*). Multiple metastatic nodules and neovascularization in metastatic lung tumor lesion (*bottom*). *B*, time profile of free SN-38 concentration in metastatic or nonmetastatic lung tissues in mice treated with NK012 (20 mg/kg/d). *Bars*, SD. Experiments were performed in tetraplicate.
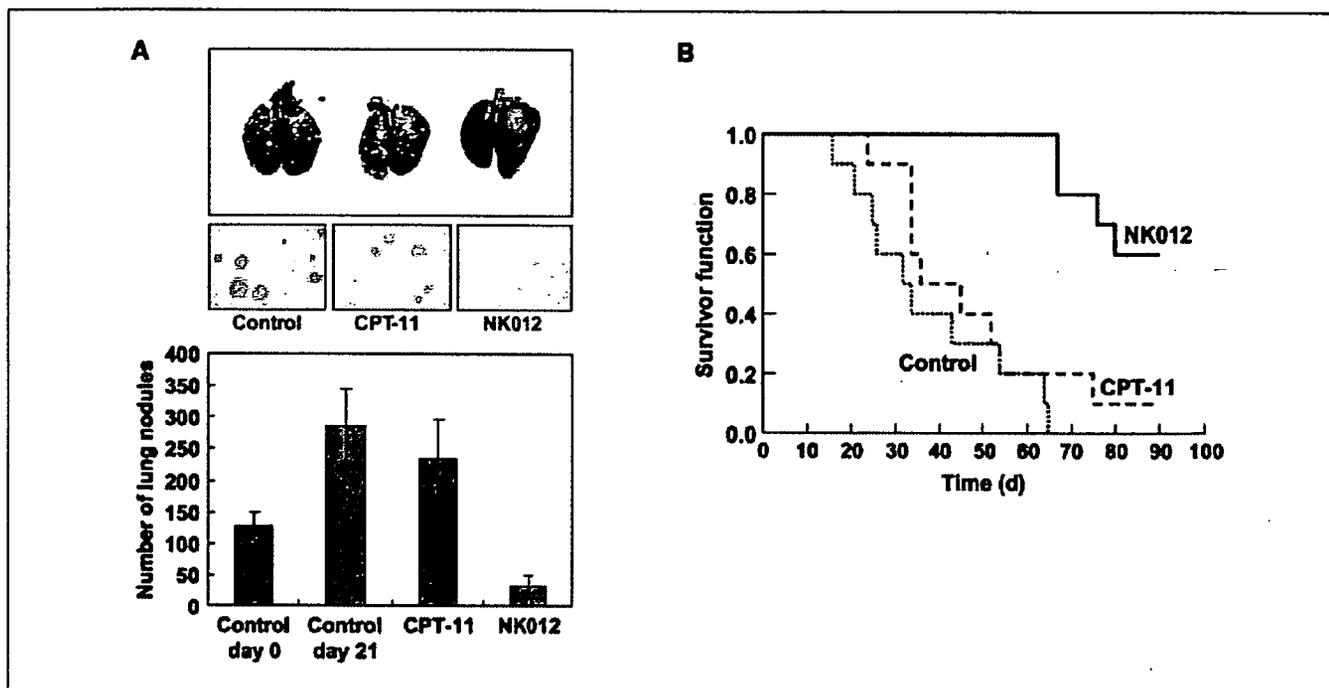
Figure 4. Treatment effect of NK012 on established pulmonary metastasis and survival. NK012 (20 mg/kg/d) and CPT-11 (30 mg/kg/d) were given i.v. to mice with established pulmonary metastasis on days 0 (7 d after Renca inoculation), 4, and 8. *A*, gross and histologic appearances of pulmonary metastases at day 21 (*top*). The metastatic nodules in each mouse were counted. Each group consisted of five mice. *B*, mice were maintained for 90 d after each treatment and survival was assessed by a Kaplan-Meier analysis. Each group consisted of five mice. Experiments were repeated twice with similar results.

the control group ($P < 0.001$), but no significant survival benefit was obtained in CPT-11 treatment group ($P = 0.239$; Fig. 4*B*). Although no severe toxic effects were observed in any mouse treated with NK012, 3 of 10 mice treated with NK012 were sacrificed during the observation period according to the 'Guidelines for Animal Experiments because their body weights had become 10% lower than those of the other mice. However, the sacrificed mice were a little bit smaller than others when they started treatment, and they showed no disseminated lung metastasis (data not shown).

Our results presented here strongly support recent findings reported by us that the macromolecular drug distribution throughout the tumor site was enhanced by the hypervascularity and hyperpermeability, and subsequently higher antitumor activity was achieved (6). We assume that conventional low molecular size anticancer agents almost disappear from the bloodstream without being subjected to the EPR effect before they can reach the target organs (solid tumor). The clinical importance of angiogenesis in human tumors has been shown in several reports indicating a positive relationship between the blood vessel density in the tumor mass and poor prognosis with chemoresistance in patients with various cancers (7-9). Furthermore, recent reports showing that anticancer agents were less active against VEGF-overexpressing tumors (10, 11) may support the idea that low-molecular drugs are not so effective in the treatment of solid tumors which are rich in blood vessels.

Our study thus far has several limitations about clarifying whether extensive angiogenesis in the tumor is an essential determinant for the susceptibility to NK012. In our ongoing study, we found that NK012 also has a striking antitumor activity against some hypovascular tumor models of human pancreatic cancer

xenografts.[5] It also remains unclear whether NK012 possesses strong antitumor activity in other metastatic sites besides the lung. It is known that the EPR effect is affected by various permeability factors, such as bradykinin (12), nitric oxide (13). and various cytokines independent of VEGF and hypervascularity (14). Among solid tumors with rapid progression potential, irregularity occurs not only in blood flow and vascular density, but also in the vascular network and anatomic architecture (15, 16), suggesting that EPR effect may be predominantly promoted in rapid-progressive tumor phenotypes and influenced by organ-specific tumor microenvironment. Hoffman and coworkers (17, 18) have developed a technique of surgical orthotopic implantation (SOI) with more clinical features of systemic and aggressive metastases than our conventional animal models. Further preclinical studies using such models as SOI might clarify cancer phenotypes and metastatic organs to which we can apply NK012 more precisely.

The results of chemotherapy in RCCs have been disappointing, as indicated by the low response proportions. However, clinical trials using gemcitabine-containing regimens have been encouraging, with major responses occurring in 5% to 17% of patients (19, 20), suggesting the possibility that chemotherapy is promising as a modality for RCC therapy if anticancer agents can be selectively delivered, released, and maintained around tumor tissues. Our current report highlights the advantages of polymeric micelle-based drug carriers like NK012 as promising modalities for treatment, rather than prevention, of disseminated RCCs with abnormal vascular architecture. The results of our ongoing phase-I

---

[5] Y. Saito, M. Yasumaga, J. Kuroda, Y. Koga, and Y. Matsumura. Unpublished data.

clinical trial and future phase-II trials of NK012 in patients with advanced solid tumors including RCC might meet or even exceed our expectations.

Acknowledgments

References

1. Matsumura Y, Maeda H. A new concept for macromolecular therapeutics in cancer chemotherapy: mechanism of tumoritropic accumulation of proteins and the antitumor agent smancs. Cancer Res 1986;46:6387-92.
2. Yokoyama M, Miyauchi M, Yamada N, et al. Characterization and anticancer activity of the micelle-forming polymeric anticancer drug adriamycin-conjugated poly(ethylene glycol)-poly(aspartic acid) block copolymer. Cancer Res 1990;50:1693-700.
3. Kataoka K, Harada A, Nagasaki Y. Block copolymer micelles for drug delivery: design, characterization and biological significance. Adv Drug Deliv Rev 2001;47:113-31.
4. Matsumura Y, Hamaguchi T, Ura T, et al. Phase I clinical trial and pharmacokinetic evaluation of NK911, a micelle-encapsulated doxorubicin. Br J Cancer 2004;91: 1775-81.
5. Hamaguchi T, Kato K, Yasui H, et al. A phase I and pharmacokinetic study of NK105, a paclitaxel-incorporating micellar nanoparticle formulation. Br J Cancer 2007;97:170-6.
6. Koizumi F, Kitagawa M, Negishi T, et al. Novel SN-38-incorporating polymeric micelles, NK012, eradicate vascular endothelial growth factor-secreting bulky tumors. Cancer Res 2006;66:10048-56.
7. Gasparini G, Harris AL. Clinical importance of the determination of tumor angiogenesis in breast carcinoma: much more than a new prognostic tool. J Clin Oncol 1995;13:765-82.
8. Takahashi Y, Kitadai Y, Bucana CD, Cleary KR, Ellis LM. Expression of vascular endothelial growth factor and its receptor, KDR, correlates with vascularity, metastasis, and proliferation of human colon cancer. Cancer Res 1995;55:3964-8.
9. Williams JK, Carlson GW, Cohen C, Derose PB, Hunter S, Jurkiewicz MJ. Tumor angiogenesis as a prognostic factor in oral cavity tumors. Am J Surg 1994;168:373-80.
10. Natsume T, Watanabe J, Koh Y, et al. Antitumor activity of TZT-1027 (Soblidotin) against vascular endothelial growth factor-secreting human lung cancer *in vivo*. Cancer Sci 2003;94:826-33.
11. Zhang L, Hannay JA, Liu J, et al. Vascular endothelial growth factor overexpression by soft tissue sarcoma cells: implications for tumor growth, metastasis, and chemoresistance. Cancer Res 2006;66:8770-8.
12. Matsumura Y, Maruo K, Kimura M, Yamamoto T, Konno T, Maeda H. Kinin-generating cascade in advanced cancer patients and *in vitro* study. Jpn J Cancer Res 1991;82:732-41.
13. Wu J, Akaike T, Hayashida K, et al. Identification of bradykinin receptors in clinical cancer specimens and murine tumor tissues. Int J Cancer 2002;98:29-35.
14. Maeda H, Fang J, Inutsuka T, Kitamoto Y. Vascular permeability enhancement in solid tumor: various factors, mechanisms involved and its implications. Int Immunopharmacol 2003;3:319-28.
15. Suzuki M, Takahashi T, Sato T. Medial regression and its functional significance in tumor-supplying host arteries. A morphometric study of hepatic arteries in human livers with hepatocellular carcinoma. Cancer 1987;59:444-50.
16. Skinner SA, Tutton PJ, O'Brien PE. Microvascular architecture of experimental colon tumors in the rat. Cancer Res 1990;50:2411-7.
17. An Z, Jiang P, Wang X, Moossa AR, Hoffman RM. Development of a high metastatic orthotopic model of human renal cell carcinoma in nude mice: benefits of fragment implantation compared to cell-suspension injection. Clin Exp Metastasis 1999;17: 265-70.
18. Hoffman RM. Orthotopic metastatic mouse models for anticancer drug discovery and evaluation: a bridge to the clinic. Invest New Drugs 1999;17:343-59.
19. Rini BI, Vogelzang NJ, Dumas MC, Wade JL III, Taber DA, Stadler WM. Phase II trial of weekly intravenous gemcitabine with continuous infusion fluorouracil in patients with metastatic renal cell cancer. J Clin Oncol 2000;18:2419-26.
20. Nanus DM, Garino A, Milowsky MI, Larkin M, Dutcher JP. Active chemotherapy for sarcomatoid and rapidly progressing renal cell carcinoma. Cancer 2004; 101:1545-51.

● *Original Contribution*

HERPES SIMPLEX VIRUS THYMIDINE KINASE-MEDIATED SUICIDE GENE THERAPY USING NANO/MICROBUBBLES AND ULTRASOUND

Atsuko Aoi,*[†] Yukiko Watanabe,* Shiro Mori,[‡] Masahiko Takahashi,[†]
Georges Vassaux,[§‖] and Tetsuya Kodama*

*Biomedical Engineering Research Organization, Tohoku University, [†]Graduate School of Dentistry, Tohoku
University, [‡]Tohoku University Hospital, Sendai, Japan; and [§]INSERM CIC-004, [‖]Institut des maladies de
l'Appareil Digestif, CHU Hotel Dieu, Nantes, France

Abstract—A physical method using ultrasound (US) and nano/microbubbles (NBs) can deliver exogenous molecules noninvasively into a specific target site. In this study, we evaluated the application of this technology to cancer gene therapy using prodrug activation therapy. Low-intensity pulsed ultrasound (1 MHz; 1.3 W/cm^2) and NBs were used to transduce the herpes simplex thymidine kinase (HSVtk) gene *in vitro*, leading to gene transfer. The addition of ganciclovir (GCV) to the transduced cells led to HSVtk/GCV-dependent cell death mediated by apoptosis. This technology was then assessed *in vivo*, using mice bearing subcutaneous tumors (1 MHz; 3.0 W/cm^2). Gene transfer to the tumor, measured by luciferase activity, was transient, with a peak of expression 24 h after transduction, and decreased at 48 h, demonstrating the transient nature of US/NB-mediated gene transfer. The therapeutic potential of this approach was evaluated through repeated intratumoral gene delivery using US/NB-mediated transfer of the HSVtk gene, followed by recurrent administration of GCV, using two different experimental treatment protocols. In both cases, dramatic reductions of the tumor size by a factor of four were observed. Altogether, these data demonstrate the potential of US/NB as a new physical gene delivery method for cancer gene therapy. (E-mail: kodama@tubero.tohoku.ac.jp) © 2008 World Federation for Ultrasound in Medicine & Biology.

Key Words: Membrane permeability, *In-vivo* imaging, Molecular delivery, Cancer gene therapy.

INTRODUCTION

Cancer therapy based on gene delivery requires highly efficient molecular delivery methods into a specific target site. One of the physical methods of gene delivery exploits nano/microbubbles (NBs) combined with ultrasound (US). Nano/microbubbles are encapsulated gas bubbles with a radius of <5 μm. The shell membrane consists of albumin, lipid or polymer. The inside gas comprises either air or perfluorocarbons (large molecules have a small diffusion efficiency into liquid, resulting in increased bubble life time) (Chomas et al. 2001; Harvey et al. 2001). These bubbles are not only used as US contrast agent to identify and delineate cardiac anatomy, such as thrombi or clot formation, but they are also used for evaluation of blood pool and blood flow at the microvascular level (Lindner 2004). The mechanical index

(MI, defined as the peak negative pressure divided by the square root of the US frequency) of US used in clinical application is 0.05 to 1.9 (McCulloch et al. 2000) and NBs collapse at MI = 0.3 to 0.5 (Ammi et al. 2006; Chen et al. 1995; Wu and Tong 1998). The impulsive pressures generated by either the collapse of NBs or cavitation bubbles created by the collapse of NBs are able to induce a transient permeabilization of cells, followed by the entry of exogenous molecules into cells. This method is not toxic and nonimmunogenic and can be combined with chemotherapy (Pitt et al. 2004).

Suicide gene therapy involves transfer into cancer cells of a gene capable of converting nontoxic prodrugs into cytotoxic drugs. One of the most common approaches uses the herpes simplex virus thymidine kinase (HSVtk) gene combined with the prodrug ganciclovir (GCV). The nucleoside analogue GCV is phosphorylated 1,000 times less efficiently by eukaryotic thymidine kinases and experimentally, *in vivo*, GCV is only phosphorylated by cells producing the virus enzyme HSVtk

Address correspondence to: Tetsuya Kodama, Ph.D., Professor, Biomedical Engineering Research Organization, Tohoku University, 2–1 Seiryo-machi, Aoba-ku, Sendai 980–8575, Japan. E-mail: kodama@tubero.tohoku.ac.jp

(Keller et al. 1981; Oliver et al. 1985). The product of the reaction (GCV-MP) is then further phosphorylated to GCV-diphosphate (GCV-DP) and GCV-triphosphate (GCV-TP) by endogenous cellular kinases. GCV-TP inhibits competitively the incorporation of dGTP into DNA (Mesnil and Yamasaki 2000), resulting in cell death (Fillat et al. 2003; Mesnil and Yamasaki 2000). Apoptosis has been suggested to be involved in the cell death, which may occur by a pathway independent of p53 (Wallace et al. 1996). In fact, it has been reported that cell lines with mutant p53 expressing HSVtk were not resistant to GCV (Vassaux and Martin-Duque 2004; Wallace et al. 1996; Yoon et al. 1999). Cytotoxicity is observed not only in HSVtk-positive cells but also in neighboring HSVtk-negative cells as a result of the bystander effect. HSVtk-negative cells show cytotoxicity in vitro when the population of cultured cells contained only 10% HSVtk-positive cells (Freeman et al. 1993). This bystander effect is regarded as a transfer phenomenon of the toxic metabolites of GCV from HSVtk-positive cells to HSVtk-negative cell, in which gap junctional intercellular communication (GJIC) appears crucial.

In the present report, we evaluated the potential of US and NBs as a physical method of gene transfer in cancer gene therapy using the HSVtk/GCV system as a therapeutic agent.

MATERIALS AND METHODS

Nano/microbubbles

Two types of NBs, Optison™ (Amersham Health PLC, Oslo, Norway) and lipid-micelle bubbles were used. Both bubbles provided very similar physical chemical properties (size distribution and ζ potential). A report on the systematic comparison of the two reagents is currently in preparation. Optison is an octafluoropropane (C_3F_8)-filled albumin microspheres that has a mean diameter between 3.0 and 4.5 μm (max. 32.0 μm). In this study, the mean concentration was set to the arithmetic average of 6.5 × 10^8 bubbles/mL. Lipid-micelle bubbles were created in an aqueous dispersion of 2 mg/mL 1,2-distearoyl-sn-glycero-3-phosphocholine (DSPC) (Avanti Polar Lipids, Alabaster, AL, USA) and 1 mg/mL polyethleneglycol-40 stearate (PEG) (Sigma-Aldrich Co., St. Louis, MO, USA) using a 20-kHz sonicator (Vibra Cell, Sonics & Materials, Inc., Danbury, CT, USA) in the presence of C_3F_8 gas (Aoi et al. 2006). The theoretically calculated concentration was 1.6 × 10^{10} bubbles/mL. The lipid bubble surface that comprised lipid molecules was confirmed by staining lipid molecules with 3 μM FM1-43 (553 nm, Abs: 570 nm, Em., Molecular Probe Inc, Eugene, OR, USA) under an inverted microscope (IX81, Olympus Co., Tokyo, Japan). The bubble size distribution was determined by using a laser diffraction particle size analyzer (particle range of 0.6 nm-7 μm, ELSZ-2, Otsuka Electronics Co. Ltd, Osaka, Japan). The peak diameters expressed in terms of the size distribution of Optison and lipid bubbles were 1689 ± 150 nm (n = 4) and 1272 ± 163 nm (n = 7), respectively. Because the volume distribution is proportional to the third power of the size, the peak of the size distribution tends to be measured as a smaller value than that of the volume distribution. The ζ potential of the bubbles was measured by the ELSZ-2 in phosphate-buffered saline without Mg_{2+} and Ca_{2+} (PBS). Zeta potential refers to the electrostatic potential generated by the accumulation of ions at the surface of a bubble that is organized into an electrical double layer. The ζ potential of the Optison and lipid bubble, was -36.9 ± 2.70 mV (n = 3) and -4.11 ± 0.74 mV (n = 4), respectively, indicating that Optison have larger mutual impulsive forces and higher stability compared with the lipid bubbles. In our previous experiments, there were no significant differences in in-vitro gene activity between Optison and lipid micelle bubbles (data not shown). In the following experiments, lipid-micelle bubbles and Optison were used for in-vitro and in-vivo experiments, respectively.

Cell preparation

Human lung carcinoma (A549) and murine colon carcinoma (colon26, which was abbreviated as C26 in the text) were obtained from the Cell Resource Center for Biomedical Research, Institute of Development, Aging and Cancer, Tohoku University, Sendai, Japan. Murine breast carcinoma (EMT6) cells were obtained from the American Type Culture Collection (Manassas, VA, USA). Murine breast carcinoma cells (EMT6-luc) stably expressing the firefly luciferase gene were prepared by transfected pEGFPLuc (BD Biosciences, Franklin Lakes, NJ, USA) and Lipofectin Transfer Reagent (Invitrogen, Carlsbad, CA, USA). Human colon carcinoma cells (HT29) were obtained from Cancer Research UK (London, UK), and human colon carcinoma cells (HT29-luc) stably expressing the firefly luciferase gene were obtained from Xenogen (Alameda, CA, USA). A549, C26, HT29 and HT29-luc cells were cultured under standard conditions in RPMI 1640 supplemented with 10% heat-inactivated fetal bovine serum (FBS) (Invitrogen) and 1% L-glutamine-penicillin-streptomycin (Sigma-Aldrich, St. Louis, MO, USA), whereas EMT6 cells and EMT6-luc were cultured in DMEM (Sigma-Aldrich) medium with the same supplements. Cells cultured in a 10-cm culture dish were maintained in a humidified incubator at 37° C under an atmosphere of 5% CO_2 and 95% air.

Plasmids

The luciferase reporter vector pGL3-control (Promega, Madison, WI, USA), which expresses luciferase from SV40 promoter, pGV24 vector in which HSV*tk* expression is driven by the ERBB2 promoter (Vassaux et al. 1999) and pRS303 that does not have any transgene expressed, were used as mock plasmid. pGV24 and pRS303 were referred to as pHSV*tk* and pMock, respectively.

Ultrasound

Two 1-MHz submersible US probes (Fuji Ceramics Co., Fujinomiya, Japan), 12 and 38 mm in diameter, were used for *in-vitro* and *in-vivo* experiments, respectively. Each probe was located in a test chamber (380 × 250 × 130 mm³) filled with tap water. Each frequency was generated by a multifunction synthesizer (WF1946A; NF Co., Yokohama, Japan), amplified with a high-speed bipolar amplifier (HSA4101; NF Co.). The pressure values were measured by a PVDF needle-hydrophone (PVDF-Z44–1000; Specialty Engineering Associates, Soquel, CA, USA) at a stand-off distance of 1 mm from the transducer surface using a stage control system (Mark-204-MS, Sigma Koki, Tokyo, Japan). The signals from both the amplifier and the hydrophone were recorded into a digital phosphor oscilloscope (Wave Surfer 454, 500 MHz, 1 mol/LΩ (16 pF), LeCroy Co., Chestnut, NY, USA).

In-vitro *transfection by ultrasound and nanobubbles*

In-vitro studies were performed in accordance with the Tohoku University ethical guidelines. A549 (1×10^4 cells/well), HT29 (1×10^4 cells/well), C26 (2×10^4 cells/well) and EMT6 (2×10^4 cells/well) cells were seeded in 24-well plates in complete media at 37° C in a 5% CO_2 incubator. The next day, the medium was replaced with fresh media (200 μL), containing pMock (4 μg/mL) or pHSV*tk* (4 μg/mL) with and without NBs (10% v/v). The 24-well plates were located just above the US probe in a test chamber filled with tap water and exposed to the optimized US (intensity: 1.3 W/cm², duty ratio: 50%, number of pulse: 2000, exposure time: 10s). The surface of the media was disturbed by US, thus we ignored the effect of standing waves on gene expression. Because cells were seeded into wells alternately, neighboring wells were not exposed to ultrasound at the same time. The plates were incubated for 1 h at 37° C in a 5% CO_2 incubator, supplemented with 800 μL of complete media and then incubated for another 24 h at 37° C in a 5% CO_2 incubator.

In-vitro *sensitivity to GCV assays*

Twenty-four hours after transfection, the media was replaced with complete media (1 mL) containing GCV (0.1–1000 μg/mL, molecular weight 255.2; F. Hoffman-La Roche Ltd., Basel, Switzerland). The plates were incubated for another three to five days at 37° C in a 5% CO_2 incubator. Survival fractions were measured by MTT assay (Kodama et al. 2003; Martinico et al. 2006). Each experiment consisted of six to 15 samples receiving US + NB + GCV with HSV*tk* (or Mock) and six to 15 control samples receiving US and NB. For each experiment, the mean % of treated samples was divided by the mean % of control samples to give a survival fraction. The mean of six to 15 survival fractions was calculated for each condition. The survival fraction of each cell line was measured at the GCV concentration where the highest statistical significant was obtained.

RT-PCR

The total RNAs were reverse-transcribed using the RNA PCR Kit (AMV) (Takara Bio Inc., Tokyo, Japan) according to the manufacturer's instructions (1 μg of total RNA was used). The cDNAs obtained were then subjected to polymerase chain reaction (PCR) amplification (3 min at 94 °C, and 35 cycles of denaturation 95 °C for 60 s, annealing 58.4 °C for 60 s and extension 72 °C for 60 s, followed by 5 min of extension 72 °C) with either HSV*tk*-specific primers (5'-AACAATGGGCAT-GCCTTATGC-3'; 5'-TTATACAGGTCGCCGTTGGGG-3', with an expected PCR product of 540 bp) or β-actin–specific primers (5'-CTGTCTGGCGGCACCACCAT-3'; 5'-GCAACTAAGTCATAGTCCGC-3', with an expected PCR product of 254 bp). The PCR products were then separated on a 2% agarose gel.

Apoptotic assay

Apoptotic cells were detected by fluorescence microscopy (DAPI staining) and TUNEL assay. For DAPI staining, cells incubated in the presence of GCV (10 μg/mL) for 24 h after the treatment of US+NB+ HSV*tk* were stained with DAPI solution (100 ng/mL). For TUNEL assay, cells were harvested at 48 h after treatment, fixed in 4% (w/v) paraformaldehyde with PBS and then washed with PBS and stored in 70% ethanol at –20° C for at least 30 min. The ethanol solution was subsequently removed after centrifugation, and cells were treated with the enzyme terminal deoxynucleotidyl transferase and FITC-labeled dUTP using the Mebstain apoptosis kit from MBL (Nagoya, Japan) according to the manufacturer's protocol. FITC-labeled cells were measured by flow cytometry (FACSCalibur, Becton Dickinson, San Jose, CA, USA). A total of 10,000 events per sample were collected in list mode, and data were analyzed with Cell Quest software (Becton Dickinson). Fluorescence data were collected by using 488-nm excitation from a 15-mW air-cooled argon-ion laser. The emission was collected through a 530 ± 30-nm band-pass

filter (FL1-H). In addition, forward-light scatter (FSC-H) and side-light scatter (SSC-H) data were collected for each sample. The mean fluorescence uptake was defined as the number of the events multiplied by the geometric mean of the channel number.

Monitoring gene transfer in vivo

Tumors were induced by subcutaneous injection of 1 × 10⁶ of either EMT6 or C26 cells in 6 week-old BALB/c mice (two mice for each cell line, two tumors/ mouse). Ten-microgram DNA (1 μg/μL) of pGL3-control with NBs (15 μL) and saline (5 μL) were injected intratumorly for a total volume of 30 μL (day 0). The tumor was immersed into water and exposed to US at 3.0 W/cm² for 60 s. At day 1 and day 2, mice were anesthetized with isoflurane, subsequently received i.p. injection with luciferin (150 μg/g body weight) and were placed on the in-vivo imaging system. The bioluminescence signals were monitored using an IVIS100 (Xenogen Corp., Alameda, CA, USA).

Bioluminescence intensity and tumor volume

In-vivo studies were performed in accordance with the Tohoku University ethical guidelines. In this study,

Table 1. Number of samples per condition in Fig. 1.

	Control	☐	▨	■
A549	6	6	6	6
HT29	6	6	6	6
C26	15	14	15	9
EMT6	12	10	9	12

A549: human lung adenocarcinoma cell, HT29; human colon carcinoma cell, C26: murine colon carcinoma cell, EMT6: murine mammary carcinoma cell. US: ultrasound, NB: nano/microbubbles, GCV: ganciclovir, Mock: pRS303 that does not have any transgene expressed, HSVtk: pGV24 vector in which the herpes simplex thymidine kinase (HSVtk) gene expression is driven by the ERBB2 promoter. ☐: US + NB + GCV, ▨: Mock + US + NB + GCV, ■: HSVtk + US + NB + GCV.

11 BALB/c mice (8- to 10-week-old) were used. Tumors were induced by subcutaneous injection of 0.25 × 10⁶/ 100 μL/site to 1 × 10⁶/100 μL/site of EMT6-luc cells into both flanks (two tumors/mouse). The intensity and volume were measured from two to 23 days after inoculation. Each mouse was anesthetized with isoflurane and subsequently received i.p. injection with luciferin (150 μg/g body weight), and placed on the in-vivo imaging system to measure the bioluminescence signals. The tumor volume was measured with a caliper and calculated according to the formula $(\pi/6) \times (\text{width})^2 \times (\text{length})$.

Therapeutic effect in vivo

Two types of experiments were conduced for low- and high-invasion tumors. Low-invasion case (subcutaneous tumor): SCID mice received subcutaneous injec-
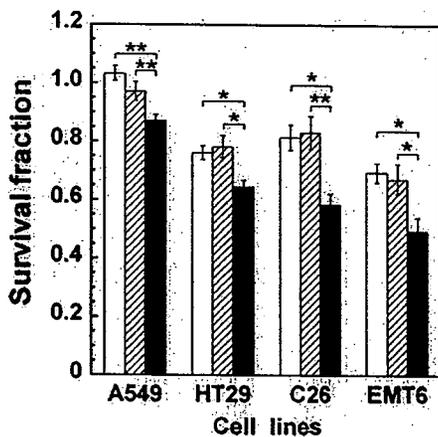

Fig. 1. Effect of NBs and US on GCV cytotoxicity in HSVtk-expressing cancer cells. Survival fractions were measured by MTT assay. Table 1 shows the number of samples used in Fig. 1. Each experiment consisted of six to 15 samples receiving US + NB + GCV with HSVtk (or Mock) and six to 15 control samples receiving US and NB. For each experiment, the mean % of treated samples was divided by the mean % of control samples to give a survival fraction. The mean of six to 15 survival fractions was calculated for each condition. ☐: US + NB + GCV; ▨: Mock + US + NB + GCV, ■: HSVtk + US + NB + GCV. A549 at day five with 5 μg/mL GCV, HT29 at day four with 10 μg/mL GCV, C26 examined at day three with 100 μg/mL GCV and EMT6 at day three with GCV 100 μg/mL). Ultrasound intensity was 1.3 W/cm². NB: lipid-micelle bubble. Bars represent the mean ± SEM. *p < 0.05; **p < 0.01.
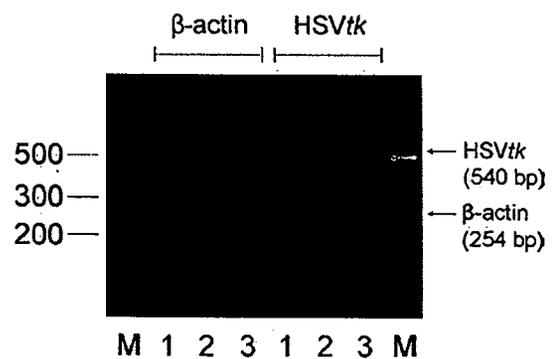

Fig. 2. Gel electrophoretic analysis of a RT-PCR reaction of HSVtk gene expressed in A549 cells induced by NBs and US. NB: lipid-micelle bubble. Lane M: 100-bp size ladder. Lane 1: cell alone. Lane 2: Mock + US + NB. Lane 3: HSVtk + US + NB. Total RNA was extracted from the cultures (pool of 6 wells) at 24 h after transfection, reverse-transcribed and amplified. The HSVtk-amplified fragment is 540 bp. The housekeeping gene, β-actin was 254 kb. This is a representative example from two separate experiments.

tions of 1 × 10⁶/100 μL/site HT29-luc cells on each flank site on day 0 (2 tumors/mouse; 2 mice for control and mock groups, 3 mice for HSV*tk* group). The injection site was detectable more than three days after the injection because the skin color was changed. In addition, the site was given an India ink tattoo temporally. On days three, six, and nine, a total volume of 30 μL including 10 μL pHSV*tk* (1 μg/μg) (or pMock (1 μg/μg)) with 15 μL of NBs and 5 μL of saline was injected into the tumor site and the tumor was sonicated at 3.0 W/cm² for 60 s (2 tumors/mouse, 2 mice). On the same days, mice were imaged with the IVIS imaging system. From day four, GCV was administered i.p. to each mouse every day. High-invasion case (intramuscular tumor): 17 SCID mice received i.m. injection of 5 × 10⁵/30 μL/site HT29-luc cells in each tibialis anterior muscle on day 0.

Every three days after day two, pHSV*tk* was injected into the tumor with US/NB method and GCV was injected i.p. five times per week for four weeks after day three. Eight control mice (3 mice [1 tumor/mouse] and 5 mice [2 tumors/mouse]) and three mice (1 tumor/mouse from HSV*tk* group) were culled on day 10 and the remaining six mice (3 mice in each group) were culled on day 30. On day 10, one or two tumors per each control mouse and one tumor for all mice in the treatment group were homogenized. On day 30, one tumor per mouse for all mice (3 mice in each group) was homogenized. All homogenized tumor samples were used to measure luciferase activity biochemically using a luciferase assay kit (Promega). Protein content was calculated using albumin standard curves (BCA Protein Assay Kit, Pierce, Rockford, IL, USA). Luciferase activity was converted to RLU/mg protein. Increase in the tissue temperature because of attenuation of US was ignored because the US frequency was 1 MHz and the depth of solid tumors (skin and muscle tumors) from the skin was <5 mm.

Statistical analysis

All measurements are expressed as mean ± SEM (standard error of mean). An overall difference between the groups was determined by one-way analysis of variance (ANOVA). Comparisons between two samples were made using Student's *t*-test. When the one-way
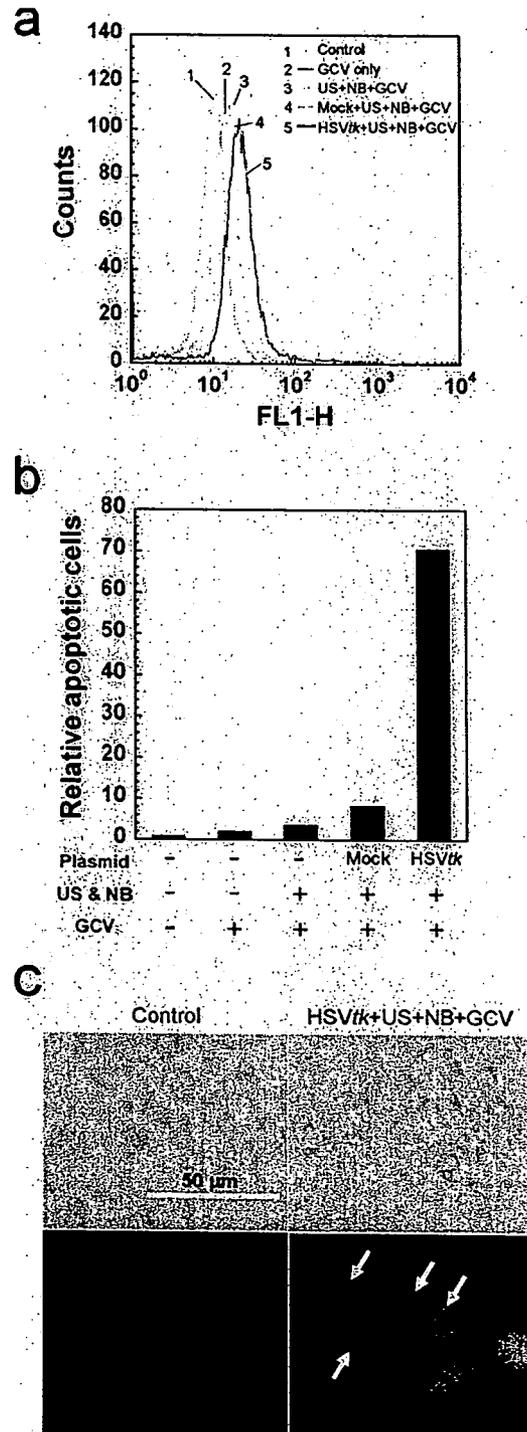

Fig. 3. Apoptosis analysis. (a) Histogram shows DNA fragmentation by TUNEL assay in A549 cells, measured at 48 h after the GCV treatment. GCV was 10 μg/mL. 1: Control (cell alone); 2: GCV alone; 3: US + NB + GCV; 4: Mock + US + NB + GCV; 5: HSV*tk* + US + NB + GCV. Cells were shifted to the higher fluorescence intensity values with increasing the number. (b) Number of TUNEL-positive cells obtained in Fig. 3a, expressed in bar chart. The emission was collected through a 530 ± 30-nm band-pass filter (FL1-H). The mean fluorescence uptake was defined as the number of the events multiplied by the geometric mean of the channel number, which was normalized with that of control cells alone. (c) Apoptosis in A549 cells was investigated by DAPI staining morphologically. A549 cells was incubated in the presence of GCV (10 μg/mL) for 24 h after the treatment of US + NB + HSV*tk*. NB: lipid-micelle bubble.
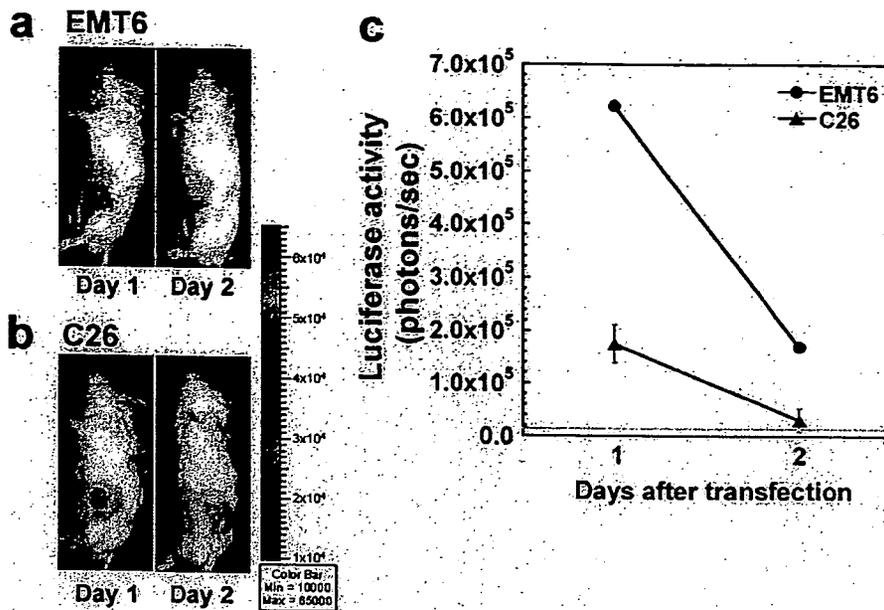
Fig. 4. Kinetics of luciferase gene expression in tumor-bearing BALB/c mice after gene transfection with US and NB. Two cell lines, EMT6 and C26, were used. Each cell line was injected into both flanks per mouse. Two mice were used for each cell line. (a, b) Representative images showing luciferase gene expression in the tumor of each cell on days 1 and 2. Color bar units represent photons/s/cm^2. (a) EMT6 cells. Gene expression was detected in only one flank. (b) C26 cells. Gene expression was detected in three flanks. (c) Luciferase activity with elapsed time. Background level (1.46 × 10^4 photons/s). Gene expression vanished in two days after the transfection by the US/NB method. Ultrasound intensity was 3.0 W/cm^2. NB: Optison. Bars represent the mean ± SEM.

ANOVA was significant and there were three samples, the differences between each group were estimated using the Tukey-Kramer test. The differences were considered to be significant at $p < 0.05$.

Mock + US + NB, whereas the fragment (254 bp) of β-actin was observed for each condition.

RESULTS

Gene transfer and GCV-mediated cytotoxicity in vitro

We first demonstrated that the combination of NBs with US could induce the sensitivity of different cell lines (A549, HT29, C26, EMT6) to killing by GCV *in vitro*. Because the sensitivity to GCV depends on the type of cells, the concentration of GCV and the assay day of cytotoxicity were varied for each cell line. MTT assay showed that exposure of US alone to cells (without NBs) did not induce cell damage (>0.95) (data not shown). Therefore, we compared HSV*tk* + US + NB + GCV with US +NB + GCV and Mock + US +NB + GCV. The MTT assay of four cell lines shows the significant cytotoxicity to GCV with HSV*tk* + US + NB + GCV compared with the control groups (Fig. 1). The sample numbers for each condition were shown in Table 1. HSV*tk* gene transfer was confirmed by RT-PCR (Fig. 2), where samples obtained under the same condition of Fig. 1 were analyzed. HSV*tk* + US + NB shows the single clear fragment (540 bp) compared with cell alone and
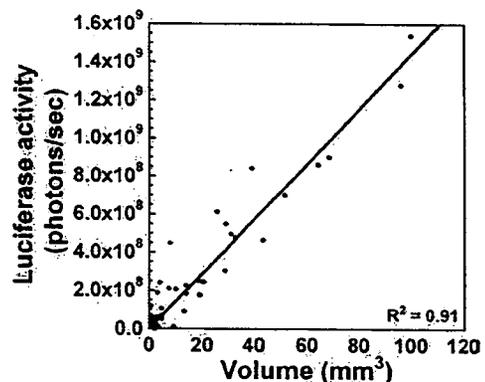

Fig. 5. The relationship between the light intensity and solid volume of EMT6-luc cells stably expressing the firefly luciferase gene. Cells were injected subcutaneously in mouse flanks (2 tumors/mouse). The number of mice and tumors was seven and 11, respectively. The intensity was measured from two to 23 days after inoculation. The volume was measured with a caliper. Tumor volume was calculated according to the formula ($\pi/6$) × (width)^2 × (length).
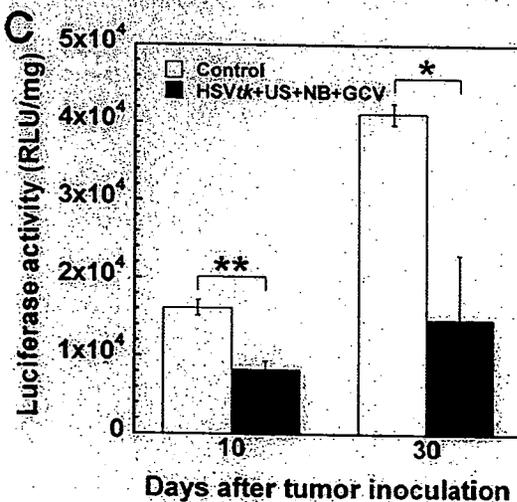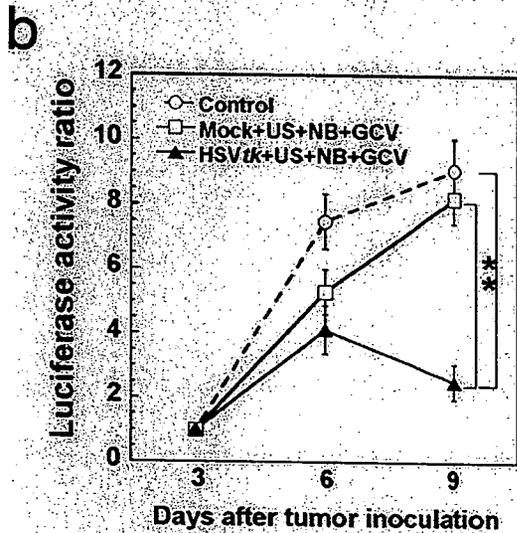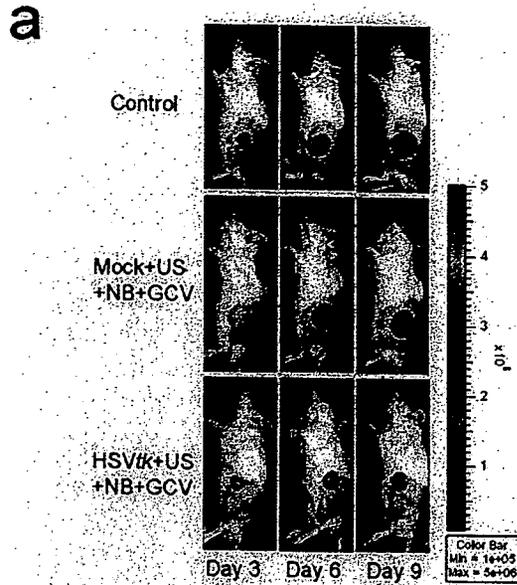
Apoptosis

We investigated whether the cytotoxicity was induced *via* apoptosis. Flow cytometry analysis of the TUNEL assay for A549 cells shows the curve in HSV*tk* + US + NB + GCV shifts largely to the right compared with other control groups, suggesting that dUTP labeled with biotin binds to DNA strand break (Fig. 3a). Figure 3b shows the histogram of Fig. 3a, indicating that the uptake of dUTP for HSV*tk* + US + NB + GCV is enhanced by a factor of 7 compared with Mock + US + NB + GCV. Because dUTP is also incorporated into DNA strands of necrotic cells, we stained A549 cells with DAPI staining and investigated the induction of apoptosis in the cells morphologically (Fig. 3c). As seen in Fig. 3c, apoptotic characteristics such as plasma membrane convolution, cytoplasmic blebbing, and nuclear condensation and fragmentation are observed; thus apoptosis is induced by the effect of HSV*tk*/GCV with the US/NB method.

Gene transfer in vivo: *Marker study*

The US/NB method induces a transient gene expression. First we investigated the kinetics of gene expression in tumor-bearing BALB/c mice by the US/NB method and determined the administration times by the US + NB. Two cell lines, EMT6 (Fig. 4a) and C26 (Fig. 4b), were used. Luciferase gene expression in these different solid tumors showed the same kinetics. The maximum luciferase activity was obtained at day one after transfection and reduced to the background level at day two (Fig. 4c). From these results, we delivered pHSV*tk* into tumor-bearing SCID mice by the US/NB method two to three times per week to maintain a high HSV*tk* gene expression level.

Fig. 6. Effect of GCV upon intratumoral HSV*tk* gene transfer with ultrasound and NB. (a, b) Data obtained with HT29-luc cells $(1 \times 10^6/100 \ \mu L$ of saline) injected subcutaneously into SCID mice. (a) Representative images showing bioluminescence in the tumors of each group on days three, six and nine. Color bar units represent photons/s/cm^2. (b) Bioluminescence was quantified at days three, six and nine. Statistical analysis was performed with the Tukey-Kramer test. Ultrasound intensity was 3.0 W/cm^2. NB: Optison. Bars represent the mean ± SEM; **$p < 0.01$. (c) Tumors were induced by i.m. injection of HT29-luc cells $(5 \times 10^5/30 \ \mu L$ of saline) into each tibialis anterior muscle of SCID mice for each group on day zero, and from day three, GCV 40 (mg/kg) diluted in PBS was given daily. Tumors were removed and homogenized at 10 and 30 d. The luciferase activity was measured with a luminometer. Statistical analysis was performed by using Student's *t*-test. Ultrasound intensity was 3.0 W/cm^2. NB: Optison. Bars represent the mean ± SEM; *$p < 0.05$, **$p < 0.01$.

Bioluminescence intensity and tumor volume

We investigated the linearity between the bioluminescence intensity and the solid tumor volume. EMT6-luc cells were injected subcutaneously. The cells allowed us to measure the size of the tumor because the cells are relatively low invasive and the boundary of the generated solid tumor is identified relatively easily. The volume was measured with a caliper and the light intensity was obtained with the *in-vivo* imaging system. As seen in Fig. 5, the linearity between the bioluminescence intensity and the tumor volume was kept up to 100 mm^3 (the width of solid tumor was <6 mm). Therefore, tumors with a volume <100 mm^3 were analyzed with the *in-vivo* imaging system in the experiment.

Therapeutic effects in vivo

Based on Figs. 4 and 5, we investigated the antitumor effect of US/NB-mediated HSV*tk* gene transfer to HT29-luc bearing SCID mice for the first experiment. The cells were injected and grown subcutaneously. The tumors were transduced three days after tumor cell inoculation and gene transfer was repeated on days six and nine. Daily i.p. injection of GCV (40 mg/kg) was administered from day four. Figure 6a and b show that a very significant reduction in tumor volume in mice treated with HSV*tk*, US, NB and GCV compared with control groups indicate that the US/NB method has therapeutic effects.

In clinical practice, most tumors may not be distinguished clearly from normal tissue as they are infiltrated into normal tissue. In a second experiment, HT29-luc cells were injected into the TA muscle and the tumors treated by US/NB-mediated gene transfer and GCV. US/NB-mediated HSV*tk* gene transfer was performed every three days from day four and GCV (40 mg/kg) was administered five times per week. Bioluminescence of the tumors *in vivo*, as well as enzymatic activity on biopsies, was measured (Fig. 6c). Luciferase activity measured biochemically on day 10 shows a statistical difference in tumor burden between control and HSV*tk* + US + NB + GCV. Furthermore, there was a statistical difference in tumor burden on day 30, with mice treated with HSV*tk* + US + NB + GCV, showing a 4 times reduction in tumor burden compared with control (Fig. 6c). During the course of these experiments, no weight reduction was observed in treated and untreated mice. Altogether, these results demonstrate the potential of HSV*tk* + US + NB + GCV treatment.

DISCUSSION

The concept of the molecular delivery method using US and NB is to induce a transient membrane permeability of cells, followed by the entry of exogenous

molecules into the cells. It has been suggested that the impulsive pressures generated by either the collapse of NBs or cavitation bubbles created by the collapse of NBs are able to induce a transient permeabilization of cells, followed by the entry of exogenous molecules into cells. Gene or oligodeoxynucleotide transfer using NB and US has already been reported (Kodama et al. 2005, 2006a, 2006b; Takahashi et al. 2007), but in this manuscript we demonstrate that this technology can be applied successfully to cancer gene therapy. *In-vitro* US/NB-mediated transfer of the HSV*tk* gene (Fig. 2) and incubation of the transduced cells with GCV leads to reduced cell survival (Fig. 1). This DNA-dependent cell kill was achieved through apoptosis (Fig. 3), as expected from the well-established mode of action of HSV*tk*/GCV (Freeman et al. 1993; Hamel et al. 1996; Wallace et al. 1996; Yoon et al. 1999).

In the present *in-vivo* study, we evaluated the *in-vivo* cytotoxicity by US/NB-mediated gene transfer by bioluminescence. The linearity between the intensity of bioluminescence and the tumor volume was kept up to a volume of 100 mm^3 (the width was <6 mm) (Fig. 5), where tumor volume was calculated according to the formula $(\pi/6) \times (\text{width})^2 \times (\text{length})$. In general, tumor size correlates closely with light intensity (Mendel et al. 2003; Soling et al. 2004). In agreement with our observations, Soling et al. (2004) reported that tumor size is not correlated with light intensity when the tumor becomes large (>12–15 mm in diameter) based on the same equation. In fact, in our recent studies, we have found that bioluminescence measurement collected using the IVIS imaging system showed a great correlation between mean bioluminescence and mean 3D tumor volume quantified using high frequency ultrasound imaging system (data not shown).

In-vivo gene expression was detectable 24 h after transfection and was dramatically reduced 48 h later (Fig. 4), highlighting the transient nature of US/NB-mediated gene transfer. This kinetics is in sharp contrast with adenovirus-mediated (Groot-Wassink et al. 2002, 2004) or nonviral gene transfer (Harada-Shiba et al. 2002; Yoshino et al. 2006), which usually lead to a maximal level of expression 48 h after transduction and can last several days at least. The transient nature of US/NB-mediated gene delivery has implications when applied in the context of pro-drug activation therapy: gene delivery must be repeated and the pro-drug must be provided shortly after transduction. This transient expression is likely to be the result of rapid plasmid DNA degradation.

In many *in-vivo* experiments, solid tumors are induced subcutaneously and used as therapeutic targets. However, therapeutic effects need to be considered using tumors infiltrated into normal tissues. In the present

experiment, we provided data demonstrating therapeutic effects of US/NB-mediated gene transfer for two types of tumors. One was subcutaneous (low-invasive) and the other was i.m. tumors (high-invasive). Figure 6 clearly shows the efficacy of the treatment with low-invasive and (Fig. 6a and b) high-invasive tumors (Fig. 6c) by US/NB-mediated gene transfer.

Considering the efficacy of the current version of NBs presented in this report and the potential for chemical modifications of the shell material (Li et al. 2003; Wang et al. 2005), and for incorporation of specific ligands in the shell membrane to enhance the tissue-specificity against the target site (Lindner 2004), the system associating NB, DNA and US could provide an alternative option to viral cancer gene therapy.

REFERENCES

Ammi AY, Cleveland RO, Mamou J, Wang GI, Bridal SL, O'Brien WD. Ultrasonic contrast agent shell rupture detected by inertial cavitation and rebound signals. IEEE Trans Ultrason Ferroelectr Freq Control 2006;53:126–136.

Aoi A, Konno K, Shinohara F, Mori S, Vassaux G, Kodama T. Effects of anti-cancer drug of cisplatin using nanobubbles and ultrasound. Ultrasound Med Biol 2006;32:280.

Chen SH, Chen XH, Wang Y, Kosai K, Finegold MJ, Rich SS, Woo SL. Combination gene therapy for liver metastasis of colon carcinoma *in vivo*. Proc Natl Acad Sci U S A 1995;92:2577–2581.

Chomas JE, Dayton P, Allen J, Morgan K, Ferrara KW. Mechanisms of contrast agent destruction. IEEE Trans Ultrason Ferroelectr Freq Control 2001;48:232–248.

Fillat C, Carrio M, Cascante A, Sangro B. Suicide gene therapy mediated by the Herpes Simplex virus thymidine kinase gene/ Ganciclovir system: Fifteen years of application. Curr Gene Ther 2003;3:13–26.

Freeman SM, Abboud CN, Whartenby KA, Packman CH, Koeplin DS, Moolten FL, Abraham GN. The "bystander effect": Tumor regression when a fraction of the tumor mass is genetically modified. Cancer Res 1993;53:5274–5283.

Groot-Wassink T, Aboagye EO, Glaser M, Lemoine NR, Vassaux G. Adenovirus biodistribution and noninvasive imaging of gene expression *in vivo* by positron emission tomography using human sodium/iodide symporter as reporter gene. Hum Gene Ther 2002; 13:1723–1735.

Groot-Wassink T, Aboagye EO, Wang Y, Lemoine NR, Keith WN, Vassaux G. Noninvasive imaging of the transcriptional activities of human telomerase promoter fragments in mice. Cancer Res 2004; 64:4906–4911.

Hamel W, Magnelli L, Chiarugi VP, Israel MA. Herpes simplex virus thymidine kinase/ganciclovir-mediated apoptotic death of bystander cells. Cancer Res 1996;56:2697–2702.

Harada-Shiba M, Yamauchi K, Harada A, Takamisawa I, Shimokado K, Kataoka K. Polyion complex micelles as vectors in gene therapy—Pharmacokinetics and *in vivo* gene transfer. Gene Ther 2002; 9:407–414.

Harvey CJ, Blomley MJ, Eckersley RJ, Cosgrove DO. Developments in ultrasound contrast media. Eur Radiol 2001;11:675–689.

Keller PM, Fyfe JA, Beauchamp L, Lubbers CM, Furman PA, Schaeffer HJ, Elion GB. Enzymatic phosphorylation of acyclic nucleoside analogs and correlations with antiherpetic activities. Biochem Pharmacol 1981;30:3071–3077.

Kodama T, Aoi A, Vassaux G, Mori S, Morikawa H, Koshiyama K, Yano T, Fujikawa S, Tomita Y. A non-invasive tissue-specific molecular delivery method of cancer gene therapy. Minim Invasive Ther Allied Technol 2006a;15:226–229.

Kodama T, Doukas AG, Hamblin MR. Delivery of ribosome-inactivating protein toxin into cancer cells with shock waves. Cancer Lett 2003;189:69–75.

Kodama T, Tan PH, Offiah I, Partridge T, Cook T, George AJ, Blomley MJ. Delivery of oligodeoxynucleotides into human saphenous veins and the adjunct effect of ultrasound and microbubbles. Ultrasound Med Biol 2005;31:1683–1691.

Kodama T, Tomita Y, Koshiyama K, Blomley MJ. Transfection effect of microbubbles on cells in superposed ultrasound waves and behavior of cavitation bubble. Ultrasound Med Biol 2006b;32: 905–914.

Li T, Tachibana K, Kuroki M, Kuroki M. Gene transfer with echo-enhanced contrast agents: Comparison between Albunex, Optison, and Levovist in mice—Initial results. Radiology 2003;229:423–428.

Lindner JR. Microbubbles in medical imaging: current applications and future directions. Nat Rev Drug Discov 2004;3:527–532.

Martinico SC, Jezzard S, Sturt NJ, Michils G, Tejpar S, Phillips RK, Vassaux G. Assessment of endostatin gene therapy for familial adenomatous polyposis-related desmoid tumors. Cancer Res 2006; 66:8233–8240.

McCulloch M, Gresser C, Moos S, Odabashian J, Jasper S, Bednarz J, Burgess P, Carney D, Moore V, Sisk E, Waggoner A, Witt S, Adams D. l. Ultrasound contrast physics: A series on contrast echocardiography, article 3. J Am Soc Echocardiogr 2000;13:959–967.

Mendel DB, Laird AD, Xin X, Louie SG, Christensen JG, Li G, Schreck RE, Abrams TJ, Ngai TJ, Lee LB, Murray LJ, Carver J, Chan E, Moss KG, Haznedar JO, Sukbuntherng J, Blake RA, Sun L, Tang C, Miller T, Shirazian S, McMahon G, Cherrington JM. In vivo antitumor activity of SU11248, a novel tyrosine kinase inhibitor targeting vascular endothelial growth factor and platelet-derived growth factor receptors: Determination of a pharmacokinetic/ pharmacodynamic relationship. Clin Cancer Res 2003;9:327–337.

Mesnil M, Yamasaki H. Bystander effect in herpes simplex virus-thymidine kinase/ganciclovir cancer gene therapy: Role of gap-junctional intercellular communication. Cancer Res 2000;60:3989–3999.

Oliver S, Bubley G, Crumpacker C. Inhibition of HSV-transformed murine cells by nucleoside analogs, 2'-NDG and 2'-nor-cGMP: Mechanisms of inhibition and reversal by exogenous nucleosides. Virology 1985;145:84–93.

Pitt WG, Husseini GA, Staples BJ. Ultrasonic drug delivery—A general review. Expert Opin Drug Deliv 2004;1:37–56.

Soling A, Theiss C, Jungmichel S, Rainov NG. A dual function fusion protein of Herpes simplex virus type 1 thymidine kinase and firefly luciferase for noninvasive *in vivo* imaging of gene therapy in malignant glioma. Genet Vaccines Ther 2004;2:7.

Takahashi M, Kido K, Aoi A, Furukawa H, Ono M, Kodama T. Spinal gene transfer using ultrasound and microbubbles. J Control Release 2007;117:267–272.

Vassaux G, Hurst HC, Lemoine NR. Insulation of a conditionally expressed transgene in an adenoviral vector. Gene Ther 1999;6: 1192–1197.

Vassaux G, Martin-Duque P. Use of suicide genes for cancer gene therapy: Study of the different approaches. Expert Opin Biol Ther 2004;4:519–530.

Wallace H, Clarke AR, Harrison DJ, Hooper ML, Bishop JO. Ganci-
clovir-induced ablation non-proliferating thyrocytes expressing
herpesvirus thymidine kinase occurs by p53-independent apoptosis.
Oncogene 1996;13:55–61.

Wang X, Liang HD, Dong B, Lu QL, Blomley MJ. Gene transfer with
microbubble ultrasound and plasmid DNA into skeletal muscle of
mice: Comparison between commercially available microbubble
contrast agents. Radiology 2005;237:224–229.

Wu J, Tong J. Experimental study of stability of a contrast agent in an
ultrasound field. Ultrasound Med Biol 1998;24:257–265.

Yoon SS, Carroll NM, Chiocca EA, Tanabe KK. Influence of p53 on
herpes simplex virus type 1 vectors for cancer gene therapy. J
Gastrointest Surg 1999;3:34–48.

Yoshino H, Hashizume K, Kobayashi E. Naked plasmid DNA transfer
to the porcine liver using rapid injection with large volume. Gene
Ther 2006;13:1696–1702.

Spinal gene transfer using ultrasound and microbubbles

Masahiko Takahashi [a,*], Kanta Kido [a], Atsuko Aoi [a,b], Hiroshi Furukawa [c],
Masao Ono [c], Tetsuya Kodama [b]

[a] Department of Oral Medicine and Surgery, Tohoku University Graduate School of Dentistry, Japan
[b] Department of Nanomedicine, Tohoku University Biomedical Engineering Research Organization, Japan
[c] Department of Pathology, Tohoku University Graduate School of Medicine, Japan

Abstract

Spinal gene therapy is a promising option for treating various spinal-related disorders. Several previous studies using viral vectors reported successful transfer of therapeutic genes into the spinal nerve system. However, because of the considerable immunogenicity related to the use of viruses, non-viral gene transfer still needs to be developed. One possible approach is the combined use of ultrasound and echo-contrast microbubbles. The present study shows that this method can be applied for targeted intrathecal gene delivery. We intrathecally injected a mixture of plasmid-DNA encoded with luciferase and commercially available albumin microbubbles by needle puncture at the lower lumbar intervertebral space in mice. Subsequent percutaneous ultrasonication on the lumbar vertebrae significantly enhanced the luciferase expression, analyzed by imaging luciferin bioluminescence, in the dorsal meningeal cells at the insonated region. No apparent neurological damages were induced by the present spinal interventions. In addition to the general benefits of the combined use of ultrasound and microbubbles, our approach can offer some advantages specific to spinal gene transfection including minimal invasiveness of simple percutaneous dural puncture, targetability due to the limited access of ultrasound waves through anatomical apertures of the vertebrae, and possible paracrine delivery of therapeutic molecules to the spinal nerve system.
© 2006 Elsevier B.V. All rights reserved.

Keywords: Gene therapy; Spinal disorder; Intrathecal delivery; Ultrasound; Microbubble

1. Introduction

Spinal gene transfer is expected to become a promising option for treating various spinal-related disorders including nerve injury, degenerative diseases, neoplasm, and chronic pain [1,2]. To date, the most widely used vehicles for gene delivery are viral vectors. Recent animal studies using adenovirus vectors indicated that direct spinal injection of specific growth-factor genes achieved functional recovery after acute spinal cord injury [3–5]. The feasibility of virus-mediated gene transfer to treat chronic pain has been also explored using the precursor genes of endogenous opioids [6,7]. The targeted spinal tissues for the

opioid-gene transfer can be both meningeal and parenchyma cells. Among the utilized viral vectors that are mostly derived either from adenoviruses, adeno-associated viruses, herpes simplex viruses or retroviruses [8], herpes vectors may be the most promising for antinociceptive gene therapy because of its high selectivity to primary afferent neurons [2,9].

Despite such experimental successes in virus-mediated gene delivery, however, alternative non-viral transgene applications need to be developed because the clinical use of viral vectors is limited by such possible disadvantages as immunogenic properties, inflammatory responses, and the difficulty of producing large amounts of pure virus. In this context, it has been reported recently that the emission of high-pressure ultrasound in combination with echo-contrast agents, microbubbles, can facilitate gene transfection into cells [10]. Possible explanations for the mechanisms include the production of transient pores on the cell membranes as well as an increase in the

* Corresponding author. Division of Dento-oral Anesthesiology, Department of Oral Medicine and Surgery, Tohoku University Graduate School of Dentistry, 4-1 Seiryo-machi, Aoba-ku, Sendai 980-8575, Japan. Tel./fax: +81 22 717 8401.
E-mail address: m-takaha@mail.tains.tohoku.ac.jp (M. Takahashi).

membrane fluidity by impulsive pressures raised when micro-bubbles are disrupted by ultrasound [11,12]. The combined use of microbubbles and ultrasound for gene delivery has several advantages including low toxicity, low immunogenicity, low invasiveness, high target selectivity, and repeatable applicability [11]. In the present study, we focused on spinal gene delivery and demonstrated that percutaneous ultrasonication in combination with intrathecal microbubbles facilitated gene transfection in spinal meningeal cells in mice.

2. Materials and methods

2.1. Animals

The study was approved by the Animal Care Committee of Tohoku University Graduate School of Medicine. Male inbred BALB/c mice were purchased from the institutional breeding facilities at 5–6 weeks of age and maintained in an antigen- and virus-free room (22 ± 1 °C, $60 \pm 10\%$ relative humidity, 12 h/12 h light/dark cycle, food and water ad libitum). The mice were studied at 7–8 weeks of age.

2.2. Plasmid DNA

pCMV-luciferase-GL3 (pcLuc-GL3: 7.4 kb) was constructed by cloning the luciferase gene from the pGL3-Control Vector (Promega Corp., Madison, WI, USA) into pcDNA3 (5.4 kb) (Invitrogen, San Diego, CA, USA) at the HindIII and BamHI sites. Plasmid DNA was purified with a QIAGEN plasmid isolation kit (QIAGEN, Hilden, Germany) and prepared at a final concentration of 1 mg/ml.

2.3. Intrathecal transfection of plasmid DNA

Mice were anesthetized with an intraperitoneal injection of sodium pentobarbital (80 mg/kg) and immobilized in a prone position on an acrylic plate. Intrathecal access was accomplished by percutaneous lumbar puncture through the 4/5th or 5/6th intervertebral space using a 27-gauge stainless-steel needle according to the Hylden and Wilcox technique with modification [13]. Dural penetration of the needle was confirmed by inspecting tail flicks of the mice. A total volume of 10 μl containing 5 μg plasmid and commercially available albumin-coated octa-fluoropropane gas microbubbles (MB), Optison™ (Amersham Health, Oslo, Norway; $5-8 \times 10^8$/ml, 3–4.5 μm in diameter), in phosphate buffered saline at a final MB concentration either 0, 20, or 50 v/v% was then injected slowly into the intrathecal space using a 50-μl microsyringe (Hamilton, Bonaduz, GR, Switzerland). A mixture of the plasmid with MB was prepared by gentle hand shaking immediately before injection. Immediately after the intrathecal injection, the mice were placed at a vertical position in a 37 °C water bath and dorsally insonated for 1 min at the vertebral region that had been injected using an ultrasound-emitting transducer (6 mm in diameter; Fuji Ceramics Co., Fujinomiya, Japan). The ultrasound (US) parameters used were as follows: central frequency, 950 kHz; duty ratio, 20%; the average intensity per cross section, 1.3 W/cm²; acoustic pressure at a standoff distance of 1 mm from the transducer surface, 0.6 MPa; energy, 2.4 J/cm². After the insonation, the mice were dried and kept under a heat lamp until recovery from anesthesia.

2.4. Analysis of luciferase activity

Mice were killed by neck dislocation under deep anesthesia with isoflurane at 1, 3, 7 days after transfection of the luciferase gene. The spinal cord was harvested en bloc at the level of the lower thoracic to sacral region by careful dissection of the vertebrae and placed on a dish plate. Subsequently, the tissue was fully covered with Luciferin 30 mg in 1 ml PBS (Promega Co., Madison, WI, USA). Luciferin bioluminescence was immediately quantified as the luciferase activity using an in vivo imaging system (IVIS™, Xenogen Co., Alameda, CA, USA) [14].

2.5. Immunohistochemistry

The harvested spinal cords were preserved in 10% PFA for 4 h and then embedded in paraffin and sectioned. Sections (4 μm thickness) were evaluated for the presence of luciferase protein by immunostaining. The sections were deparaffinized in xylene for 5 min 3×, rehydrated through graded ethanol and equilibrated in PBS. The sections were incubated in 3% H_2O_2 for 30 min to dampen endogenous peroxidase activity. They were incubated for 30 min at room temperature with 10% normal goat serum (Nichirei Biosciences Inc., Tokyo) to reduce nonspecific protein binding. After a wash in PBS, the sections were incubated with biotin-labeled rabbit anti-luciferase antibody (0.5 g/ml) (Cortex Biochem, San Leandro, CA, USA) overnight at 4 °C. The following day, after three washes in PBS, immunoreactivity was detected using an anti-rabbit IgG Histofine SAB-PO(M) kit (Nichirei Biosciences Inc., Tokyo, Japan) and diaminobenzidine (DAB) as a chromogen according to the manufacturer's protocols. After color development, the spinal cord sections were counterstained with hematoxylin and were then dehydrated, cleared, and mounted on slides.

2.6. Assessment of post-transfectional spinal injury

2.6.1. Thermal nociception
For assessing the nociceptive responses to thermal stimuli after the intrathecal procedure, the paw withdrawal latencies following exposure to infra-red radiant heat were determined [15] using a commercial device (7370-Planter Test, Ugo Basille, Comerio, Italy) three days after the gene transfection. Mice were placed in a clear plastic chamber (210 mm × 105 mm × 130 mm) with a glass floor and allowed to acclimate for at least 5 min. After the acclimation period, radiant heat was projected to the hind paw and time count was started. The heat projection was made through a 5 mm × 10 mm aperture in the top of a movable case containing the radiant heat source that was positioned under the glass floor directly beneath the paw. The radiant heat source consisted of a high intensity projecting Halogen lamp bulb (8 V–50 W) located 40 mm below the floor. The time count was stopped when the mouse withdrew its paw. Mice were tested

with three determinations each at the right and left paw and were allowed to rest for at least 30 min between each session.

2.6.2. Rotarod

For assessing motor function after the intrathecal procedure, mice were tested using a rotarod (IITC; Life Science Instrument, Woodland Hills, CA, USA) three days after the gene transfection. The rod had a diameter of 3.8 cm and was accelerated from 0 to 30 rpm over a 17.5-s period. The total time that the mice remained on the rotarod was measured. The time count was stopped when mice fell from the rod or when they rotated around completely two times without walking [16]. Mice were tested with three trials and were allowed to rest for at least 30 min between each session.

2.7. Statistical analysis

All values are expressed as mean±SEM. Statistical analysis for the spinal luciferase activities was performed by one-factor analysis of variance (ANOVA) with Fisher's protected least significant difference test (Fisher's PLSD) as a post-hoc procedure. Unpaired Student-T test was used for the behavioral evaluations. Statistical significance was defined as $p < 0.05$.

3. Results

3.1. Effects of microbubbles and ultrasound on spinal gene transfection

Fig. 1 shows representative views of luciferin bioluminescence in the mouse spinal cord obtained by the imaging system (sum of
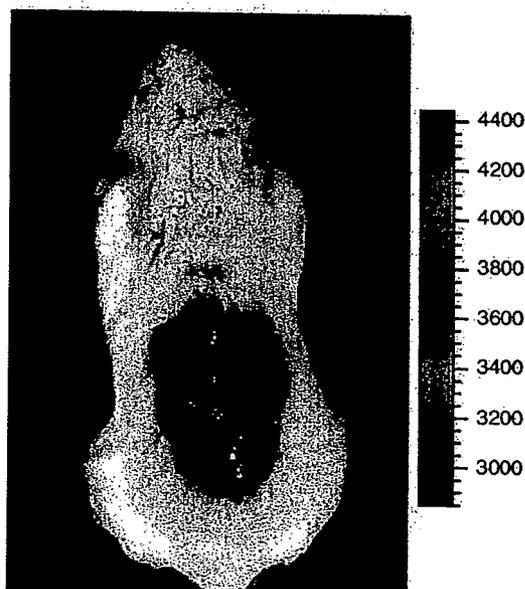

Fig. 1. Representative image showing luciferin bioluminescence (IVIS™, Xenogen Co., Alameda, CA, USA) in the spinal cord of BALB/c mice a day after the intrathecal injection of plasmid DNA and microbubbles (Optison™, Amersham Health, Oslo, Norway) followed by percutaneous ultrasonication. Imaging time is 5 min. Color bar units represent photons s^{-1} cm^{-2}.
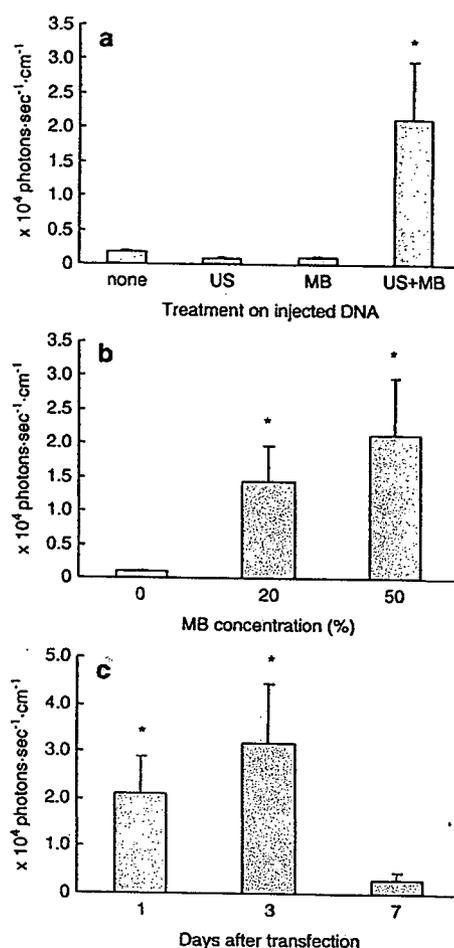

Fig. 2. Plasmid-derived spinal luciferase activity represented by luciferin bioluminescence in mice subjected to intrathecal gene delivery using ultrasound and microbubbles. The ultrasound parameters were as follows: central frequency, 950 kHz; duty ratio, 20%; the average intensity per cross section, 1.3 W/cm^2; acoustic pressure at a standoff distance of 1-mm from the transducer surface, 0.6 MPa; energy, 2.4 J/cm^2; exposure time, 1 min. (a) Treatment effects of ultrasound and 50% microbubbles one day after the application. Combined use of ultrasound and microbubbles significantly enhanced the gene transfection compared to the other treatments. (b) Effects of the microbubble concentration on the spinal gene expression. Microbubbles at concentrations of both 20 and 50% significantly enhanced the gene transfection one day after the application. No significant difference was found between the luciferase activities in mice treated with the two concentrations. (c) Time course of spinal gene expression in mice treated with ultrasound and 50% microbubbles. Luciferase activity significantly increased at 1 and 3 days after gene transfection which disappeared by the 7th day. No statistical difference was found between the gene expression at 1 and 3 days post-transfection. *$p < 0.001$. $n = 5$ in each group. US: ultrasound; MB: microbubble (Optison).

photon counts from a region of interest at 5 min is presented). The spinal luciferase activities determined one day after four different treatments (DNA alone, DNA+MB, DNA+US, and DNA+MB+US) are shown in Fig. 2a. The concentration of MB used was 50%. The luciferase activities in the treatments with DNA+MB and DNA+US were as low as that with DNA alone. In contrast, ultrasonication after the DNA+MB injection significantly increased the luciferase activity by approximately 25 fold compared to the other treatments ($p < 0.001$).

3.2. Effects of microbubble concentration on spinal gene transfection

Fig. 2b shows the spinal luciferase activities one day after ultrasonication with 0, 20, and 50% MB. While the treatment with MB significantly increased the luciferase activities ($p<0.02$), the difference between 20 and 50% MB was not significant.

3.3. Time course of spinal gene expression

The spinal luciferase activities were analyzed at 1, 3, and 7 days after the intrathecal gene transfection using US and 50% MB (Fig. 2c). The luciferase activities significantly increased at 1 and 3 days post-transfection ($p<0.02$) without an intergroup difference, and returned to a level similar to that without US (at 1 day post-treatment) after 7 days.

3.4. Histological localization of the transfected gene expression

The immunohistochemical staining revealed that luciferase expression was mostly limited to the meningeal cells in the
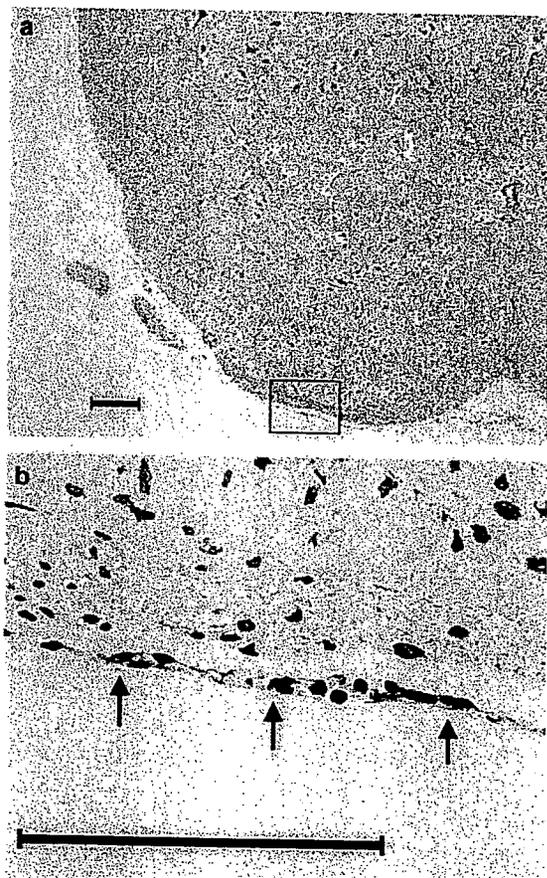

Fig. 3. Local gene expression in mouse spinal cord after intrathecal gene delivery using ultrasound and microbubbles. Expression of luciferase protein was mostly limited to the dorsal meningeal cells. (a) H&E staining in coronal sections of the lumber spinal cord. (b) Immunohistochemical localization of luciferase (arrows). Scale bar=100 μm.
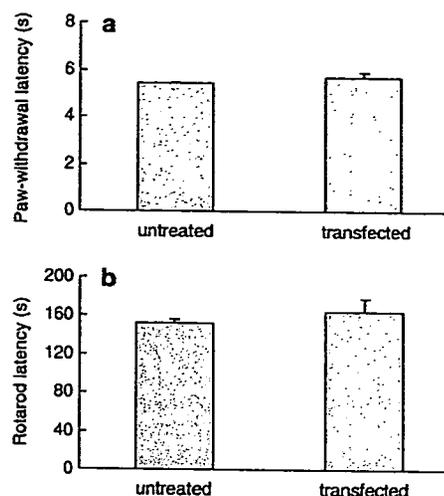

Fig. 4. Neurological evaluations of mice obtained 3 days after gene transfection using ultrasound and microbubbles (50%). (a) Paw-withdrawal latency following exposure to infra-red radiant heat. Three determinations each in the right and left hind paw were combined in each animal because the latency did not differ between the two sides. (b) Rotarod latency that represents the total time mice remained on the rotarod. Each mouse was tested with three trials. No significant difference was found compared to untreated mice in either determination. $n=4$ in each group. US: ultrasound; MB: microbubble (Optison).

dorsal surface of the spinal cord (Fig. 3). The expressing regions were likely to have been the dura mater because Fig. 3b clearly shows a positive staining for cells in a membrane structure apart from the spinal parenchyma by the space of medullary fluid. As the dura mater consists of two cell types, meningeal cell and endothelial cell, the present data cannot strictly exclude the positive staining for the endothelial cells. However, the endothelial cells are shown to be very minor cellular component, so that frequent staining may indicate expression of the gene product mainly in the meningeal cells. There were no hemorrhage or inflammatory findings in the sections.

3.5. Paw-withdrawal and rotarod latencies

Fig. 4 shows the averaged paw-withdrawal (Fig. 4a) and rotarod latencies (Fig. 4b) in untreated and transfected (DNA+ 50% MB+US) mice. Since the withdrawal latencies were not different between the right and left paw (data not shown), the data were combined in each animal. The determinations revealed no significant difference in the paw-withdrawal or rotarod latencies between the two groups, indicating that the present intervention did not affect the sensory and motor neurologic functions of the mice.

4. Discussion

The present study clearly demonstrated that percutaneous ultrasonication on an intrathecally administered mixture of plasmid-DNA and Optison facilitated the transfection of luciferase genes into the spinal meningeal cells in mice. No significant deficit was observed either in the sensory or motor neurologic functions after the procedures. In addition to the

general benefits of the combined use of ultrasound and microbubbles, our approach offers some advantages specific to spinal gene transfection. First, it requires only intrathecal needle access and percutaneous sonication that have been widely accepted in the clinical practice. Although a relatively short duration of gene expression (<7 days) was observed (Fig. 2c), the minimal invasiveness of the present surgical interventions would permit repetitive gene delivery into the spinal cord. Second, the intervertebral foramina and spaces would provide highly selective anatomical windows for ultrasound access while the vertebral bony structures would protect the spinal cord from possible excessive sonication. Although spotty gene expressions in the insonated regions would not be obvious in animals as small as the mice used in this study (Fig. 1), it can be expected that an ultrasound beam could reach the regions of the dorsal roots or the dorsal horns at targeted vertebral levels through the boneless apertures in large animals including human. This can be especially promising for transferring antinociceptive genes. Third, gene transfer into meningeal cells (Fig. 3) may be useful for topical delivery of bioactive substances into the CSF or adjacent spinal parenchyma while avoiding direct genetic modulation of parenchyma cells. Transgene-derived peptides such as growth factors, neuropeptides, or endogenous opioids that are secreted from meningeal cells would act in a paracrine manner on neurons and glias in the near vicinity, circumventing pharmacological problems related to the short half-life of the peptides or the need for high doses to achieve biological activity that could result in undesirable side effects.

Spinal gene therapy can be expected to be a promising approach to treat various spinal-related disorders. In previous animal studies, the delivery of therapeutic genes into the spinal nerve system has been mostly achieved using viral vectors [8]. However, because of the considerable disadvantages involved in using viral vectors, the development of alternative non-viral transgene techniques is needed. Cationic reagents such as cationic liposomes [17] have been developed for non-viral gene transfection. Achieving the efficient delivery of such molecules, however, to the spinal cord includes inherent difficulties. First, intrathecal injection induces diffusion of reagents into the cerebral spinal fluid (CSF), resulting in lack of target specificity. Second, since the CSF continuously circulates and replaces, a constant concentration of reagents for necessary transfection to a specific site would not be achieved. Ultrasound gene therapy is an alternative non-viral approach [18]. The insufficient transfection efficiency of simple ultrasonication can be improved by the combined use of echo-contrast microbubbles [11]. The use of ultrasound with microbubbles, which enables non-invasive, tissue-specific gene delivery, has received much interest and enhanced gene transfer has been reported in various animal tissues in vivo including heart [19], peripheral arteries [20], skeletal muscles [21], and brain [22]. Very recently, Shimamura et al. reported successful gene transfer into the rat spinal cord using ultrasound and microbubbles [23]. The authors intrathecally injected naked luciferase DNA with Optison through the 4/5th lumbar intervertebral space and applied sonication directly on the thoracic dural sac by

removing the dorsal part of the 9–10th thoracic vertebra, which resulted in the enhanced expression of luciferase in the meningeal cells in the insonated region. In contrast, we accomplished transgene expression in the meningeal cells by intrathecal injection of luciferase DNA with Optison through the lower lumbar intervertebral space, as in their study, but then employed simple transcutaneous insonation at the same lumbar region without surgical exposure of the dura. The lower invasiveness in our methodology would seem to be more clinically useful. Interestingly, the duration of transgene expression was consistently as short as a week in both studies. Although Shimamura et al. described that the short expression of transgene by single transfection would be acceptable to treat acute spinal cord trauma [23], the repeated applicability due to the lower invasiveness in the present study could enable treatments for chronic ailments. In fact, we have recently shown that successive gene expression was obtained by repeat transfection using the present ultrasound–microbubble technique [24]. Nonetheless, since gene expression for longer than 3 weeks was previously achieved by spinal electroporation via an intrathecal electrode catheter in rat meningeal cells [25,26], the present ultrasound–microbubble approach has the potential for methodological improvement to prolong the duration of transgene expression by optimizing acoustic parameters such as intensity, duty ratio, frequency, and spatial pressure distribution [12] and changing the membrane properties of microbubbles [27].

The present acoustic parameters were relatively consistent with those reported in previous studies in which ultrasound and Optison were safely used for transferring genes into nervous tissues [22,23]. Consistent with those studies, we did not find macroscopic injuries in the skin or muscles, microscopic damage in the spinal cord, or significant deficits in the spinal neurological functions. In addition, the present neurological tolerance may be alternatively explained by a characteristic of our approach, namely that the intact vertebral bony structures surrounding the intervertebral apertures limited excessive sonication of the spinal cord. Nonetheless, further optimization of the ultrasound parameters will improve the safeness of sonication on nervous tissues. The physical conditions of the microbubbles used in this study are additional issues to be discussed. First, although we evaluated only the usefulness of Optison, the possible utility and safety of microbubbles other than Optison (e.g. lipid microbubbles) for intrathecal gene transfer remains to be explored. Second, we should note that Optison at a concentration as high as 50% was used in most series of the present experiments. The reasons for this were that a trend of higher transfection efficacy was observed in the 50% group (but ns vs. 20% groups, Fig. 2b) and that no apparent neurological damage was observed in the transfected mice (Fig. 4). However, earlier studies [22,23] successfully used Optison at concentrations of 20–25% for intrathecal gene delivery in rats. It seems reasonable that intrathecal microbubbles at lower concentrations would induce fewer adverse effects while enabling an increase in the relative content of plasmid DNA in a limited volume of mixture. Therefore, it is possible that the concentration of microbubbles for intrathecal injection could be further optimized. The authors finally note

that the functional expressions of genes transfected into the spinal nerve system have not yet been examined. Further efforts using genes that are encoded with neurobioactive peptides are clearly needed to investigate the clinical usefulness of the present ultrasound–microbubble approach.

In conclusion, we demonstrated that simple percutaneous ultrasonication on intrathecally administered plasmid DNA and echo-contrast microbubbles enhanced the gene transfer into spinal meningeal cells in mice. The present approach can provide some advantages specific to spinal gene therapy including minimal invasiveness, regional targetability, and possible paracrine delivery of therapeutic molecules to the spinal nerve system. Studies including functional assessments of therapeutic gene transfer as well as the application of the techniques in larger animals will further clarify the feasibility of the present ultrasound–microbubble method in spinal gene therapy.

References

[1] J.C. Glorioso, D.J. Fink, Herpes vector-mediated gene transfer in treatment of diseases of the nervous system, Annu. Rev. Microbiol. 58 (1) (2004) 253–271.

[2] S.P. Wilson, Gene-based therapy for treatment of chronic pain, Semin. Pain Med. 1 (4) (2003) 220–226.

[3] F. Facchiano, E. Fernandez, S. Mancarella, G. Maira, M. Miscusi, D. D'Arcangelo, G. Cimino-Reale, M.L. Falchetti, M.C. Capogrossi, R. Pallini, Promotion of regeneration of corticospinal tract axons in rats with recombinant vascular endothelial growth factor alone and combined with adenovirus coding for this factor, J. Neurosurg. 97 (1) (2002) 161–168.

[4] M. Koda, M. Hashimoto, M. Murakami, K. Yoshinaga, O. Ikeda, M. Yamazaki, S. Koshizuka, T. Kamada, H. Moriya, H. Shirasawa, S. Sakao, H. Ino, Adenovirus vector-mediated in vivo gene transfer of brain-derived neurotrophic factor (BDNF) promotes rubrospinal axonal regeneration and functional recovery after complete transection of the adult rat spinal cord, J. Neurotrauma 21 (3) (2004) 329–337.

[5] X.Q. Tang, Y. Wang, Z.H. Huang, J.S. Han, Y. Wan, Adenovirus-mediated delivery of GDNF ameliorates corticospinal neuronal atrophy and motor function deficits in rats with spinal cord injury, NeuroReport 15 (3) (2004) 425–429.

[6] S.P. Wilson, D.C. Yeomans, M.A. Bender, Y. Lu, W.F. Goins, J.C. Glorioso, Antihyperalgesic effects of infection with a preproenkephalin-encoding herpes virus, Proc. Natl. Acad. Sci. U. S. A. 96 (6) (1999) 3211–3216.

[7] A.A. Finegold, A.J. Mannes, M.J. Iadarola, A paracrine paradigm for in vivo gene therapy in the central nervous system: treatment of chronic pain, Hum. Gene Ther. 10 (7) (1999) 1251–1257.

[8] M. Pohl, J. Braz, Gene therapy of pain: emerging strategies and future directions, Eur. J. Pharmacol. 429 (1–3) (2001) 39–48.

[9] M. Mata, J. Glorioso, D.J. Fink, Development of HSV-mediated gene transfer for the treatment of chronic pain, Exp. Neurol. 184 (Suppl. 1) (2003) S25–S29.

[10] P.A. Dijkmans, L.J.M. Juffermans, R.J.P. Musters, A. van Wamel, F.J. ten Cate, W. van Gilst, C.A. Visser, N. de Jong, O. Kamp, Microbubbles and ultrasound: from diagnosis to therapy, Eur. J. Echocardiog. 5 (4) (2004) 245–256.

[11] R. Bekeredjian, P.A. Graybum, R.V. Shohet, Use of ultrasound contrast agents for gene or drug delivery in cardiovascular medicine, J. Am. Coll. Cardiol. 45 (3) (2005) 329–335.

[12] T. Kodama, Y. Tomita, K. Koshiyama, M.J.K. Blomley, Transfection effect of microbubbles on cells in superposed ultrasound waves and behavior of cavitation bubble, Ultrasound Med. Biol. 32 (6) (2006) 905–914.

[13] J.L. Hylden, G.L. Wilcox, Intrathecal morphine in mice: a new technique, Eur. J. Pharmacol. 67 (2–3) (1980) 313–316.

[14] B.W. Rice, M.D. Cable, M.B. Nelson, In vivo imaging of light-emitting probes, J. Biomed. Opt. 6 (4) (2001) 432–440.

[15] K.M. Hargreaves, R. Dubner, F. Brown, C. Flores, J. Joris, A new and sensitive method for measuring thermal nociception in cutaneous hyperalgesia, Pain 32 (1) (1988) 77–88.

[16] J.D. Hommel, R.M. Sears, D. Georgescu, D.L. Simmons, R.J. DiLeone, Local gene knockdown in the brain using viral-mediated RNA interference, Nat. Med. 9 (12) (2003) 1539–1544.

[17] C.R. Dass, P.F. Choong, Selective gene delivery for cancer therapy using cationic liposomes: in vivo proof of applicability, J. Control. Release 113 (2) (2006) 155–163.

[18] C.M. Newman, A. Lawrie, A.F. Brisken, D.C. Cumberland, Ultrasound gene therapy: on the road from concept to reality, Echocardiography 18 (4) (2001) 339–347.

[19] R. Bekeredjian, S. Chen, P.A. Frenkel, P.A. Graybum, R.V. Shohet, Ultrasound-targeted microbubble destruction can repeatedly direct highly specific plasmid expression to the heart, Circulation 108 (8) (2003) 1022–1026.

[20] Y. Taniyama, K. Tachibana, K. Hiraoka, T. Namba, K. Yamasaki, N. Hashiya, M. Aoki, T. Ogihara, K. Yasufumi, R. Morishita, Local delivery of plasmid DNA into rat carotid artery using ultrasound, Circulation 105 (10) (2002) 1233–1239.

[21] Y. Taniyama, K. Tachibana, K. Hiraoka, M. Aoki, S. Yamamoto, K. Matsumoto, T. Nakamura, T. Ogihara, Y. Kaneda, R. Morishita, Development of safe and efficient novel nonviral gene transfer using ultrasound: enhancement of transfection efficiency of naked plasmid DNA in skeletal muscle, Gene Ther. 9 (6) (2002) 372–380.

[22] M. Shimamura, N. Sato, Y. Taniyama, M. Endo, H. Kurinami, M. Aoki, T. Ogihara, Y. Kaneda, R. Morishita, Development of efficient plasmid DNA transfer into adult rat central nervous system using microbubble-enhanced ultrasound, Gene Ther. 11 (20) (2004) 1532–1539.

[23] M. Shimamura, N. Sato, Y. Taniyama, H. Kurinami, H. Tanaka, T. Takami, M. Ogihara, Y. Tohyama, R. Morishita, Gene transfer into adult rat spinal cord using naked DNA and ultrasound microbubbles, J. Gene Med. 7 (11) (2005) 1468–1474.

[24] A. Aoi, K. Konno, S. Fumiaki, S. Mori, G. Vassaux, T. Kodama, HSV-tk/ GCV cytotoxic gene therapy using ultrasound and nanobubbles, Ultrasound Med. Biol. 32 (5S) (2006) 280.

[25] C.R. Lin, M.H. Tai, J.T. Cheng, A.K. Chou, J.J. Wang, P.H. Tan, M. Marsala, L.C. Yang, Electroporation for direct spinal gene transfer in rats, Neurosci. Lett. 317 (1) (2002) 1–4.

[26] T.H. Lee, L.C. Yang, A.K. Chou, P.C. Wu, C.R. Lin, C.H. Wang, J.T. Chen, C.S. Tang, In vivo electroporation of proopiomelanocortin induces analgesia in a formalin-injection pain model in rats, Pain 104 (1–2) (2003) 159–167.

[27] J.R. Lindner, Microbubbles in medical imaging: current applications and future directions, Nat. Rev. Drug Discov. 3 (6) (2004) 527–532.

Tumor specific ultrasound enhanced gene transfer *in vivo* with novel liposomal bubbles

Ryo Suzuki [a], Tomoko Takizawa [a], Yoichi Negishi [b], Naoki Utoguchi [a], Kaori Sawamura [a], Kumiko Tanaka [a], Eisuke Namai [a], Yusuke Oda [a], Yasuhiro Matsumura [c], Kazuo Maruyama [a,*]

[a] *Department of Biopharmaceutics, School of Pharmaceutical Sciences, Teikyo University, 1091-1 Suwarashi, Sagamiko, Sagamihara, Kanagawa 229-0195, Japan*
[b] *Department of Drug and Gene Delivery System, School of Pharmacy, Tokyo University of Pharmacy and Life Science, Hachioji, Tokyo, Japan*
[c] *Investigative Treatment Division, Research Center for Innovative Oncology, National Cancer Center Hospital East, Kashiwa, Chiba, Japan*

Abstract

Bubble liposomes (liposomes which entrap an ultrasound imaging gas) may constitute a unique system for delivering various molecules efficiently into mammalian cells *in vitro*. In this study, Bubble liposomes were compared with cationic lipid (CL)–DNA complexes as potential gene delivery carriers into tumor *in vivo*. The delivery of genes by Bubble liposomes depended on the intensity of the applied ultrasound. Transfection efficiency plateaued at 0.7 W/cm^2 ultrasound intensity. Bubble liposomes efficiently transferred genes into cultured cells even when the cells were exposed to ultrasound for only 1 s. In addition, Bubble liposomes could introduce the luciferase gene more effectively than CL-DNA complexes into mouse ascites tumor cells and solid tumor tissue. We conclude that the combination of Bubble liposomes and ultrasound is a minimally-invasive and tumor specific gene transfer method *in vivo*.
© 2007 Elsevier B.V. All rights reserved.

Keywords: Liposomes; Bubble liposomes; Gene delivery; Ultrasound; Cancer

1. Introduction

In cancer gene therapy, it is important to develop the easy, safe, efficient, minimally-invasive and tissue-specific technologies of gene transfer into tumor tissue. Sonoporation is a method of gene delivery with ultrasound. Ultrasound increases the permeability of the plasma membrane and reduces the thickness of the unstirred layer of the cell surface, aiding DNA entry into cells [1,2]. Preliminary studies into the utility of ultrasound for gene delivery used frequencies in the range of 20–50 kHz [1,3]. However, these frequencies are also known to induce tissue damage and cavitation if not properly controlled [4–6]. To overcome this problem, several studies have used frequencies of 1–3 MHz, intensities of 0.5–2 W/cm^2, and pulse-modulation [7–9]. In a separate approach, a combination

of therapeutic ultrasound and microbubble echo contrast agents was shown to enhance gene transfection efficiency [10–15] by effectively and directly transferring DNA into the cytosol. Microbubbles based on protein microspheres, and sugar microbubbles, are commercially available; however, although they encapsulate ultrasound contrast agents, they are too large (2–10 μm diameter) for intravascular application [16]. It has been reported that the *i.v.* injection of Optison without ultrasound exposure results in lethal embolisms in vital organs in mice [17]. Although a similar effect has not been observed in humans, it is possible that Optison can not pass through capillary vessels. Ideally, microbubbles should be smaller than red blood cells.

Liposomes can be used as drug, antigen and gene delivery carriers [18–26]. Based on liposome technology, we developed novel liposomal bubbles (Bubble liposomes) containing the ultrasound imaging gas, perfluoropropane. When coupled with ultrasound exposure, Bubble liposomes can be used as novel

---